A SIMPLE HISTORY-DEPENDENT NONWETTING-PHASE TRAPPING MODEL FOR THE TOUGH SIMULATORS

Christopher G. Patterson, Ronald W. Falta

Illinois State Geological Survey
615 E. Peabody Dr.
Champaign, IL, 61820, US
e-mail: patterc@illinois.edu

ABSTRACT

Nonwetting phase trapping by local capillary forces plays a key role in several multiphase flow processes of interest. When LNAPLs or DNAPLs are released into the subsurface, nonwetting-phase trapping causes a significant fraction of the NAPL to become immobilized in the pore space. This trapped fraction is known as the residual saturation, and it is defined as the saturation at which the relative permeability (and capillary pressure) becomes zero. Residual saturations of NAPL typically cannot be removed from the subsurface by pumping; special remediation techniques that enhance the evaporation or dissolution of the NAPL are usually required.

When supercritical CO_2 is injected into deep formations for geologic storage, similar nonwetting-phase trapping takes place, but in this setting, the trapping contributes to the long-term security of CO_2 storage. In either case, the degree to which the nonwetting phase becomes trapped is dependent on the nonwetting-phase saturation history. If the porous medium experiences high nonwetting-phase saturations (high capillary pressures), the resulting residual saturation is also large. However, prior to nonwetting-phase invasion, the nonwetting-phase residual saturation should be zero. The publicly available forward versions of the TOUGH code (e.g. TMVOC, TOUGH2-ECO2N) typically do not account for this nonwetting-phase trapping hysteresis.

The proposed trapping model adds a variable S_{nmax} to the secondary variable list to TMVOC and TOUGH2-ECO2N. S_{nmax} is defined as the maximum historical nonwetting-phase saturation within an element during a simulation. This secondary variable is fully incremented and updated during each Newton-Raphson iteration, and it is used in the relative permeability and capillary pressure subroutines to compute the nonwetting phase residual saturation, using either a linear relationship, or the equation by Land (1968). At the end of each converged time-step, S_{nmax} is stored separately, so that it can be written to the SAVE file for restarting. This approach of adding saturation hysteresis is relatively straightforward to program, it does not increase the number of model parameters in the relative permeability and capillary pressure functions, and it produces continuously differentiable functions that transition smoothly between imbibition and drainage conditions without any interpolation. A feature of the method is that the shape of the main drainage relative permeability and capillary pressure curves that result from this approach are altered from curves that use a static residual saturation.

An assessment of the new model was made by simulating an experiment by Johnston and Adamski (2005) that explored the relationship of residual- and maximum- LNAPL saturations using an undisturbed soil sample. Another assessment was made by comparing the results of the new model to an analysis by Doughty (2007) for injection and migration of a supercritical CO_2 plume in a deep storage formation. The results compare favorably and suggest that the new model can duplicate essential features of more complicated hysteretic models.

INTRODUCTION

Many multiphase flow systems involve significant nonwetting-phase trapping. For example, geologic CO_2 sequestration is a proposed method of reducing anthropogenic emissions of CO_2 by injecting CO_2 into a deep geologic unit, where all or part of the CO_2 is intended to remain. A popular method of geologic carbon

sequestration involves injecting supercritical-phase CO_2 into deep brine reservoirs. In a two-phase CO_2/brine system, the CO_2 is the nonwetting phase, and a certain fraction of the CO_2, known as the residual saturation, becomes locally trapped in the pore space due to capillary forces. This residual trapping is one of the most significant mechanisms for preventing unwanted migration of injected CO_2 (IPCC, 2005, Saadatpoor et al., 2009; Suekane et al., 2009). If the residual saturation of the CO_2 phase is low, then the CO_2 phase will tend to be mobile at low saturations, and can potentially migrate long distances under gravitational and pressure forces. Similarly, if CO_2 residual saturation is high, the CO_2 phase is only mobile at high saturations, and CO_2 phase migration will tend to be smaller due to trapping.

Environmental contaminant transport involving nonaqueous-phase liquids (NAPLs) is another area where nonwetting-phase trapping plays a key role. In a NAPL/water system, the NAPL is usually the nonwetting phase, and the residual saturation has a large effect on the NAPL migration. When NAPLs such as gasoline or chlorinated solvents are released in the environment, they migrate down through the vadose zone to the water table. Light nonaqueous-phase liquids (LNAPLs) tend to depress the water table and spread along its surface, while dense nonaqueous-phase liquids (DNAPLs) can penetrate the water table and migrate downward until a low-permeability unit is reached (Charbeneau 2007).

During supercritical CO_2 injection, or when a NAPL spill reaches the water table, the pressure difference (known as capillary pressure) between the nonwetting phase (CO_2 or NAPL) and the wetting phase (water) will drive the nonwetting phase into the largest pores of the rock first, pushing the wetting phase out of the pores (Mayer et al. 2005, Juanes et al. 2010). Smaller pores can be invaded by the nonwetting phase following increasing differential pressure between wetting and nonwetting phases (increases in capillary pressure). Once the injection stops or the spill subsides, the CO_2 or NAPL continues to migrate due to buoyancy and regional groundwater gradients. At the leading edge of the migrating CO_2 or NAPL plume, the CO_2/NAPL continues to displace the water; at the trailing edge of the plume, the water displaces the CO_2 or NAPL as capillary pressure decreases (Juanes et al., 2006). The water imbibition process leads to snap-off at the pore scale and trapping of the CO_2 or NAPL phase at the residual saturation (Juanes et al. 2010).

Several multiphase flow experiments have demonstrated that the amount of trapped nonwetting phase is dependent on the saturation history—meaning if the porous medium experiences high nonwetting-phase saturations (high capillary pressures), the resulting residual saturation is also large. Kueper et al. (1993) and Johnston and Adamski (2005) performed NAPL displacement experiments showing that the residual NAPL saturation in unconsolidated soils is approximately a linear function of the maximum historical NAPL saturation in the soil. Similarly, Krevor et al. (2011) found that the residual saturation of supercritical CO_2 in a heterogeneous rock core was a function of the maximum CO_2 saturation in the core, although the relationship between the maximum and residual saturation was nonlinear.

The amount of fluid trapped at the pore scale affects the overall mobility of the fluid in the subsurface. Where there exists both imbibition- and drainage processes, e.g., during buoyancy-driven flow of supercritical CO_2, or during NAPL transport through geologic media, the use of hysteretic values for residual saturation is critical to the prediction of fluid movement. Hysteresis has been observed experimentally in problems involving NAPLs (Lenhard and Parker 1987, Lenhard 1992, Kueper et al. 1993, Steffy et al. 1997, Johnston and Adamski 2005), and a number of hysteretic extensions to characteristic curves have been devised for predicting phase saturations in multiphase flow simulations for environmental and petroleum applications (Parker and Lenhard, 1987; Lenhard and Parker, 1987; Niemi and Bodvarsson, 1988; Kaluarachchi and Parker ,1992; Van Geel, 2002; Fagerlund et al., 2008). However, the incorporation of these hysteretic models into multiphase flow codes such as TOUGH2 (Pruess, 1999) can become relatively complex, and typically require more parameters for the hysteretic model than

for the nonhysteretic model (Doughty, 2007, Fagerlund et al., 2008).

It has been common to assume static values for the nonwetting-phase residual saturation in multiphase flow simulations. For example, the NAPL transport and remediation codes T2VOC (Falta et al., 1995) and TMVOC (Pruess and Battistelli, 2002) use a constant NAPL-phase residual saturation in the capillary pressure and relative permeability curves. Similarly, the TOUGH2-ECO2N code (Pruess, 2005; Pruess et al, 1999) used for CO_2 sequestration simulations assumes a constant value for the CO_2-phase residual saturation in the relative permeability and capillary pressure curves.

In this paper, we present a straightforward numerical method for adding hysteretic nonwetting-phase trapping, where the residual saturation in a gridblock is a dynamic function of the maximum nonwetting-phase saturation in the gridblock. This method does not require any more parameters than similar nonhysteretic models, and it produces smooth, reversible, and continuously differentiable relative permeability and capillary pressure curves under all conditions.

CHARACTERISTIC CURVES

Multiphase flow numerical models use characteristic curves to describe the interactions of the separate phases. Characteristic curves are functions describing relative permeability-saturation and capillary pressure-saturation relationships at gridblock scale, and ultimately control multiphase flow. Characteristic curves are dependent upon the properties of the material each gridblock represents.

Relative permeability curves

A relative permeability curve is a function that controls the ease at which fluids may flow in a multiphase model. Relative permeability (k_r) is a scaling factor (0-1), and it is the ratio of the effective β phase permeability, $k_{e\beta}$, to the intrinsic permeability, k.

$$k_{r\beta} = \frac{k_{e\beta}}{k} \quad , \qquad (1)$$

It is used to adapt the single phase flow Darcy equation to multiphase flow;

$$q_\beta = \frac{-k_{r\beta}k}{\mu_\beta}\left(\nabla P_\beta + \rho_\beta g \nabla z\right) \quad , \qquad (2)$$

where q_β is the darcy flux in phase β, μ_β is the viscosity of phase β, ∇P_β is the pressure gradient in phase β, ρ_β is the density of phase β, g is gravitational acceleration, and ∇z is the elevation gradient.

Nonhysteretic relative permeability curves are limited to one value of residual nonwetting-phase saturation (S_{nr}), which represents the saturation at which k_{rn} =0. Figure 1, calculated using Equation (3),

$$k_{rn}\left(S_n\right) = \sqrt{1-\bar{S}_w}\left(1-\bar{S}_w^{\,1/m}\right)^{2m} \quad , \qquad (3)$$

shows two nonhysteretic nonwetting phase relative permeability curves calculated with nonwetting phase residual saturation (S_{nr}) values of 0 and 0.25.

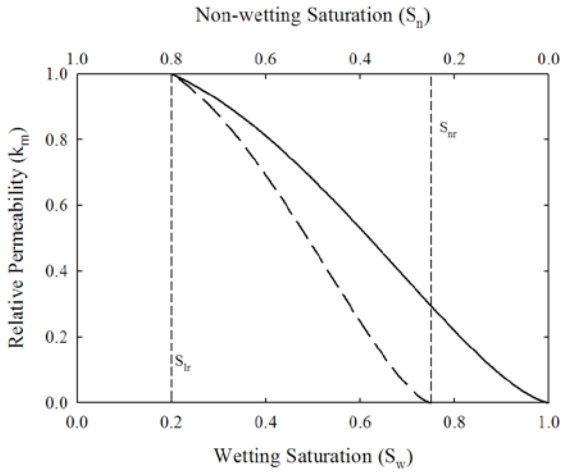

Figure 1. Examples of nonhysteretic relative permeability curves by Mualem (1976). The two curves are calculated using an S_{nr} value of 0 (solid line) and 0.25 (dashed line).

Relative permeability curves not considering hysteresis tend to underpredict the nonwetting-phase relative permeability when the phase first invades a water-filled system, and tend to overpredict the mobility if the nonwetting phase is being displaced by water (Parker and Lenhard, 1987; Lenhard and Parker, 1987; Niemi and Bodvarsson, 1988; Kaluarachchi and Parker, 1992; Fagerlund et al., 2008). If a nonhysteretic

relative permeability curve with a S_{nr} of 0.25 (i.e., dashed line in Figure 1) is used, nonwetting-phase saturation must build to 0.25 before becoming mobile. However, if the nonhysteretic relative permeability curve with an S_{nr} of 0 (i.e., solid line in Figure 1) is used, then no trapping of the nonwetting phase occurs as it leaves the pore system.

Capillary pressure curves

The capillary pressure in a two-phase system is the difference in phase pressure between the nonwetting and wetting phases. In a water-saturated system, the nonwetting phase will not enter the pores until the nonwetting-phase entry pressure (capillary pressure) is exceeded (Mayer et al. 2005). Increases in capillary pressure can drive the nonwetting phase into the smaller pores, expelling the wetting phase. Decreases in capillary pressure reverse the process. As the process is reversed, and the nonwetting phase is displaced from the media, the capillary pressure returns toward zero as the nonwetting phase residual saturation is approached. A model can only follow the capillary pressure curve as far as the residual nonwetting-phase saturation as determined from the relative permeability function, since a relative permeability of 0 deems a phase immobile.

Hysteretic characteristic curves

Nonhysteretic characteristic curves use a static value of S_{nr} and do not have the ability to capture the accurate saturation sequence for a dynamic flow process with variable trapped saturations (Mualem, 1984; Doughty, 2007). A system of pores is complex, and the saturation path upon nonwetting-phase invasion is not the same as when the nonwetting phase leaves the pores (Charbeneau, 2007). For useful estimates of residual nonwetting-phase saturation, the maximum value of nonwetting-phase saturation must be considered (Charbeneau, 2007), because regions that achieve greater nonwetting-phase saturations will retain greater residual nonwetting-phase saturations as nonwetting phase leaves the pores (Lenhard and Parker, 1987; Lenhard, 1992; Kueper et al., 1993; Steffy et al., 1997; Johnston and Adamski, 2005; Charbeneau, 2007). Hysteresis refers to irreversible saturation paths for multiphase flow interactions.

The nonwetting-phase relative permeability curve in Figure 2 is hysteretic, meaning it describes the relative permeability based not only on the current saturation, but also on the history of saturation at the respective location.

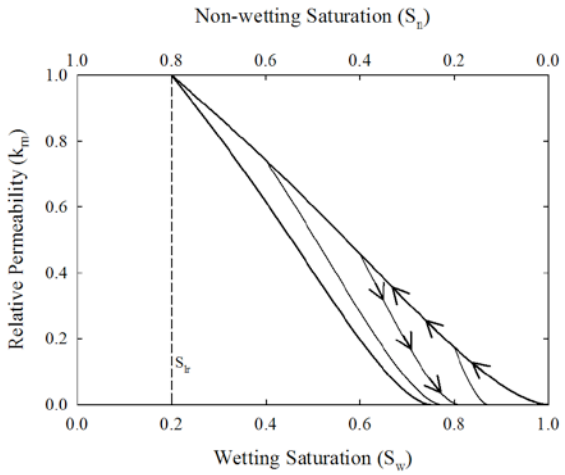

Figure 2. A hysteretic nonwetting phase relative permeability curve from Doughty (2007). The fluid saturation will follow the main drainage branch upward during nonwetting phase invasion, and will follow a secondary scanning curve downward as the nonwetting phase leaves the pore system. The path of the scanning curve depends on the turning-point saturation. This example shows multiple potential turning points each with a separate scanning curve. The value of S_{nr} is represented by $(1\text{-}S_w)$ at $k_{rn} = 0$.

Here, the amount of trapped nonwetting-phase fluid in the pores is dependent on the maximum amount of that fluid that initially entered the pores (Parker and Lenhard, 1987; Lenhard and Parker, 1987; Niemi and Bodvarsson, 1988; Kaluarachchi, 1992; Van Geel, 2002; Fagerlund et al., 2008). Note that there are multiple scanning curves for different turning-point saturations (the saturation value at the point where the nonwetting phase stops invading and starts leaving the pore system). The arrows on the curve represent the direction in which the model follows the curve during nonwetting-phase invasion and subsequent evacuation. Probably the most important aspect of hysteretic characteristic curves is the calculation of S_{nr}, represented as the value of S_n at which a scanning curve has led to a nonwetting-phase relative permeability value of zero. This varies depending on the maximum value of S_n reached during nonwet-

ting-phase invasion. Greater values of S_n reached during nonwetting-phase invasion correspond to greater values of S_{nr}.

NEW HYSTERETIC MODEL

The history-dependent trapping model was applied to the ECO2N (Pruess 2005) and TMVOC (Pruess and Battistelli 2002) codes, both of which are modules of the TOUGH2 (Pruess et at. 1999) numerical simulators developed at the Lawrence Berkeley National Laboratory. These codes are capable of simulating multidimensional fluid and heat flows of multiphase, multicomponent fluid mixtures through porous and fractured media. ECO2N is specifically designed for applications to geologic sequestration of CO_2 in saline reservoirs, capable of modeling isothermal or nonisothermal single-phase or two-phase fluid mixtures of water, CO_2, and NaCl. The chemical reactions modeled by ECO2N include equilibrium phase partitioning of water and carbon dioxide between liquid and gaseous phases, and precipitation and dissolution of solid salt. TMVOC is capable of modeling the nonisothermal flow of water, gas, and multicomponent mixtures of volatile organic chemicals (VOCs) that form a NAPL phase.

New trapping model

The new trapping model adds a variable S_{nmax} to the secondary variable list to TMVOC and TOUGH2-ECO2N. S_{nmax} is defined as the maximum historical nonwetting-phase saturation within an element during a simulation. During each Newton-Raphson iteration, S_{nmax} is updated as the primary variables change, so that the effects of the variable nonwetting trapping are fully incorporated in the Jacobian matrix. At the end of each time step, S_{nmax} is updated accordingly, and stored in a separate array. At the end of a simulation, the value of S_{nmax} in each element is written to the "SAVE" file, so that a simulation may be restarted with the historical saturation values known.

The variable S_{nmax} is used in the relative permeability and capillary pressure subroutines to compute the nonwetting-phase residual saturation. Two methods are used in this project to compute residual saturation: one trapping model is a linear relationship;

$$S_{nr} = f_r(1 - S_{w\min}) = f_r S_{n\max} \qquad (4)$$

where f_r is the slope of the linear relationship between maximum- and residual nonwetting phase saturation. The other trapping model is a popular method of estimating residual nonwetting-phase saturation from an equation by Land (1968):

$$S_{nr} = \frac{S_{n\max}}{1 + R(S_{n\max})}, \qquad (5)$$

where

$$R = \frac{1}{S_{nr\max}} - 1,$$

where $S_{nr\max}$ is the maximum possible nonwetting-phase residual saturation reached following nonwetting-phase evacuation. This is a static parameter used for the characteristic curve, determined by the maximum amount of nonwetting fluid that can be retained by the specific porous medium. S_{nr} is incorporated into the relative permeability and capillary pressure functions through the effective wetting-phase saturation, usually

$$\overline{S}_w = \frac{S_w - S_{lr}}{1 - S_{nr} - S_{lr}} \qquad (6)$$

A significant characteristic of other hysteretic models (Kaluarachchi and Parker, 1992; Doughty, 2007; Fagerlund et al., 2008) is that the derivatives of the relative permeability and the capillary pressure with respect to saturation are discontinuous at the turning points. The discontinuity is caused by an abrupt switch from a value of zero for S_{nr} while nonwetting phase is entering the element to a non-zero value for S_{nr} as nonwetting phase is leaving the element. In codes such as TOUGH2, which are based on a residual minimization method using Newton-Raphson iteration, discontinuous functions can cause a multiphase flow code to take short time steps and run very slowly (Fagerlund et al. 2008). To alleviate the numerical difficulties, the characteristic curves can be artificially smoothed as the turning points are approached (Doughty, 2007; Fagerlund et al., 2008).

Instead, we propose continuously updating the value of S_{nr} based on the S_{nmax} to ensure that the resulting curves are always smooth and continuously differentiable, leading to good numerical performance in numerical codes such as TOUGH2.

The concept of a dynamically updated residual saturation can be applied to any relative permeability or capillary-pressure function that incorporates a residual saturation. Continuously updating the value of residual nonwetting-phase saturation during nonwetting-phase invasion results in an alteration of the shape of the main drainage curve compared to traditional approaches. Therefore, adjustment of the curve parameters is necessary to match the main drainage curve with similar curves that do not incorporate the dynamic S_{nr}. In this paper, we apply our hysteresis effects to relative permeability curves by Mualem (1984) and Charbeneau (2007) and to the capillary pressure curve by van Genuchten (1980).

MODEL APPLICATIONS

NAPL displacement in a core

Johnston and Adamski (2005) measured the relationship between maximum NAPL saturation and residual NAPL saturation using unconsolidated soil cores. For their experiments, the water was the wetting phase while the decane (an LNAPL) was the nonwetting phase.

The experimental setup involved a core barrel that held a core sample with a water reservoir and a decane reservoir connected to either end. The soil core sample measured 47 mm in diameter and 50 mm in length, and was classified as a sand. A hydrophilic ceramic plate separated the core from the water reservoir, while a hydrophobic ceramic plate separated the core from the decane reservoir. The plates were placed to ensure that decane would not leak into the water reservoir and that water did not leak into the decane reservoir. The elevation of the decane reservoir remained constant to provide consistent pressure on the decane end of the cell, while the elevation of the water reservoir was varied to apply and release capillary pressure within the cell. The test cell was subjected to cycles of subsequently increasing water suction to allow decane to flow into the core. The suction was released between cycles to return capillary pressure back to zero and allow the water and decane saturations to equilibrate.
Over a span of about 90 days, six NAPL flooding cycles were performed on the soil core sample. The measurements of residual NAPL saturations showed an approximate linear relationship with the maximum NAPL saturations with a slope (f_r) of 0.394.

A one-dimensional model was set up with the modified TMVOC code to simulate this experiment. The core sample was represented by 10 gridblocks in the center of the model, the ceramic plates were each represented by 2 gridblocks on both ends of the core cells, and the reservoirs were each represented by 1 gridblock on each end of the model. Hydraulic properties of the ceramic plates and intrinsic permeability of the core sample were not measured, so estimated values were used for these parameters in the simulation (Patterson, 2011).

The gridblocks representing the core sample were initially fully saturated with water. The gridblocks representing the water and decane reservoirs were initially fully saturated with water and decane, respectively, and were held at the desired conditions—the decane reservoir gridblock kept at a constant pressure while the pressure of the water reservoir was controlled to match the experimental conditions. Actual times and values of pressure change were obtained through personal communication with Colin Johnston (2010) and were used in the pressure control for the water reservoir gridblock.

Gridblocks representing the hydrophilic plate were given a high nonwetting-phase entry pressure to repel the decane, and gridblocks representing the hydrophobic plate were given a large negative capillary pressure to repel water. The value of f_r measured by Johnston and Adamski (2005) was used to calculate S_{nr} in the hysteretic relative permeability function. The fitted van Genuchten capillary pressure parameters for the sample from Johnston and Adamski (2005) were used for the capillary pressure function (not hysteretic in this simulation), and the n value from the capillary pressure curve was used for the relative permeability curves.

Results and Discussion

The experiment was first simulated with nonhysteretic relative permeability curves to demonstrate the inaccuracy of this approach. Figure 3 shows the result of a nonhysteretic simulation run with S_{nr} value of 0. During intermittent times of applied suction, NAPL saturation returns to 0. Figure 4 shows the result of a nonhysteretic simulation run with S_{nr} value of 0.15. Obviously, the nonhysteretic relative permeability curves are unable to predict the variable trapping occurring in this experiment.

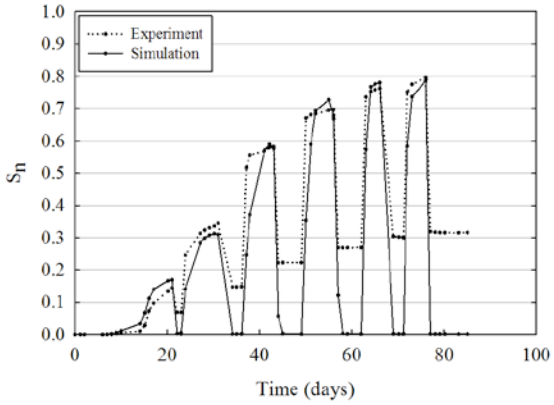

Figure 3. Nonhysteretic simulation of experiment by Johnston and Adamski (2005) using a S_{nr} value of 0.

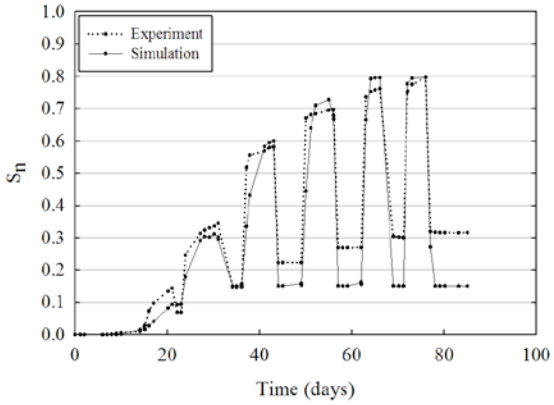

Figure 4. Nonhysteretic simulation of the experiment by Johnston and Adamski (2005) using a S_{nr} value of 0.15.

Results from the simulation using the new hysteretic relative permeability function compare favorably to the experimental results (Figure 5).

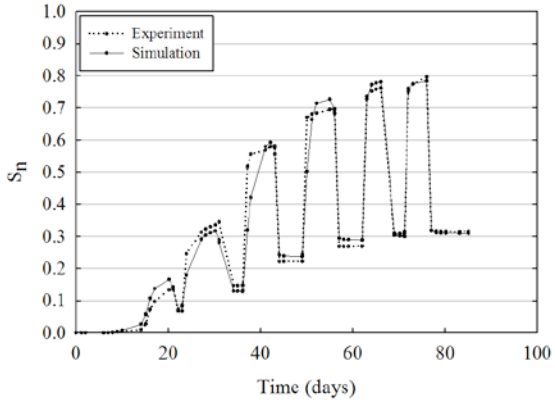

Figure 5. Simulation results for the hysteretic relative permeability model plotted with experimental results from Johnston and Adamski (2005).

Comparison with a more advanced hysteretic k_r-P_c model

The second assessment made with the new hysteretic model was to compare simulation results for a case developed by Doughty (2007) related to geologic sequestration of supercritical CO_2. Doughty's study compared the behavior of CO_2 injection simulations made using hysteretic characteristic curves with typical non-hysteretic characteristic curves.

The model scenario that was compared was a 2D cylindrical model with CO_2 injection into a 100 m thick interval with leakage through a homogeneous zone 1000 m thick. The model extended radially to 40,000 m, and was divided into 61 layers, each with 41radial gridblocks. The layers were 20 m thick except for a few thinner layers near the surface. The gridblocks were 20 m wide extending to 600 m, and then increased steadily to produce an infinite acting model. Both the injection formation and overlying formation were homogeneous, with a vertical permeability of 100 md and horizontal permeability of 200 md. The model was initially fully brine-saturated with a salinity of 100,000 ppm. The model was nonisothermal and followed a fixed geothermal gradient of 30°C/km with the surface and bottom of the model held constant at 15°C and 48°C, respectively. The simulation began by injecting 900,000 tons of CO_2 over a period of 30 days, with redistribution for 1,000 years.

To help ensure an accurate comparison of the behavior of the two hysteretic formulations, we

used the TOUGH2 input files provided by Doughty (Doughty, personal communication, 2010). The published simulations were carried using ECO2, an older version of the TOUGH2 module ECO2N. One small difference between the two modules is that ECO2N includes the density effect that CO_2 has in the aqueous phase once dissolved. This turns out to have a significant effect on the results at late simulation times. Doughty (personal communication, 2010) also provided an updated simulation using ECO2N and shared her new (unpublished) results. The comparison shown here uses these new simulations results.

Doughty (2007) employed extensions to her hysteretic formulations to ensure numerical stability. They include a power-law extension to the van Genuchten capillary pressure function to account for dissolution of trapped CO_2 and a cubic splice in the relative permeability function to smoothly connect the drainage branch to the imbibition branch (Doughty 2007). Mualem (1984) gives expressions for first- and second-order scanning curves that are implemented and expanded to third-order scanning curves by Niemi and Bodvarsson (1988). Doughty (2007) used this interpolation between scanning curves; it is recommended that the reader refer to the literature for detailed discussion on higher-order scanning curves (Niemi and Bodvarrson, 1988).

In addition to running a simulation with the new hysteretic characteristic curves, two nonhysteretic cases were simulated to further illustrate the comparison between the new hysteretic model and the hysteretic model from Doughty (2007). The same input files were used for the simulation to ensure consistency between the hysteretic and nonhysteretic models. One nonhysteretic case used a residual gas-phase saturation (S_{gr}) value of zero; the other case used an S_{gr} value of 0.25. The nonhysteretic simulations here are run with the Charbeneau (2007) relative permeability function and van Genuchten (1980) capillary pressure function. Other than the constant value of S_{gr}, model parameters are kept consistent with that of the hysteretic simulations.

The new hysteretic method used here alters the shape of the primary drainage relative permeability and capillary pressure curves. To account for this, the parameter values in our characteristic curves were adjusted so that the primary wetting-phase drainage curves were similar to those in Doughty's model.

Figures 6 and 7 show the curves fit to Doughty's capillary pressure curve and nonwetting-phase relative permeability curve, respectively. Table 1 shows both the fitted parameters used for our hysteretic capillary pressure curve and the parameters used in Doughty's hysteretic capillary pressure curve. Table 2 shows both the fitted parameters used for our hysteretic nonwetting-phase relative permeability curve and the parameters used in Doughty's hysteretic nonwetting-phase relative permeability curve.

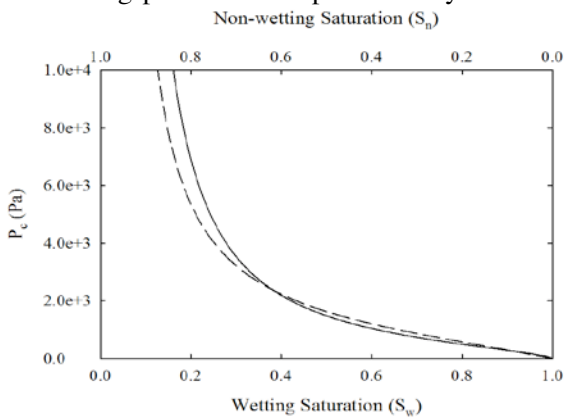

Figure 6. Main wetting-phase drainage capillary pressure curve based on van Genuchten (1980) (dashed line) that best fit the main wetting-phase drainage capillary pressure curve (solid line) from Doughty (2007).

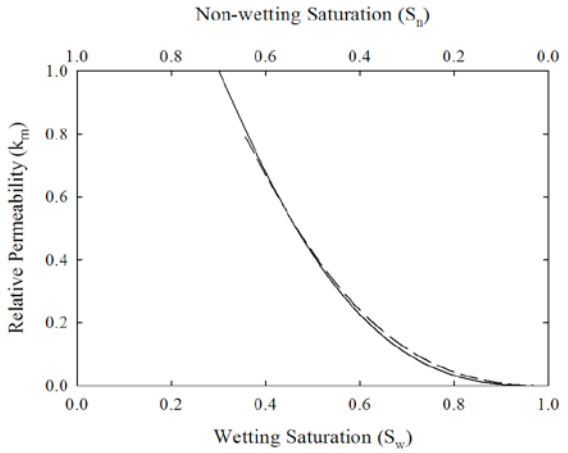

Figure 7. Primary drainage nonwetting-phase relative permeability (dashed) that best fit the relative permeability curve (solid line) from Doughty (2007).

Table 1. Hysteretic capillary-pressure-curve parameters for both the fitted curve and the curve used in Doughty (2007).

Model parameter	Fitted value	Doughty (2007) value
n	2.94	1.7
S_{lr}	0.2	0.03
α	0.53933	0.737293
S_{gr} max	0.25	0.25

Figure 8 shows the results from the nonhysteretic simulations: one case with an S_{gr} value of zero and another case with an S_{gr} value of 0.25. The first case (S_{gr} = 0) predicts a completely mobile CO_2 plume, and by 1,000 years all of the CO_2 has leaked to the surface. The second case (S_{gr} = 0.25) shows a fairly immobile plume; the CO_2 never reaches the surface and remains trapped indefinitely.

Table 2. Hysteretic relative permeability curve parameters for both the fitted curve and the curve used in Doughty (2007).

Model parameter	Fitted value	Doughty (2007) value
n	2.083	12
S_{lr}	0.3	0.3
S_{grmax}	0.25	0.25

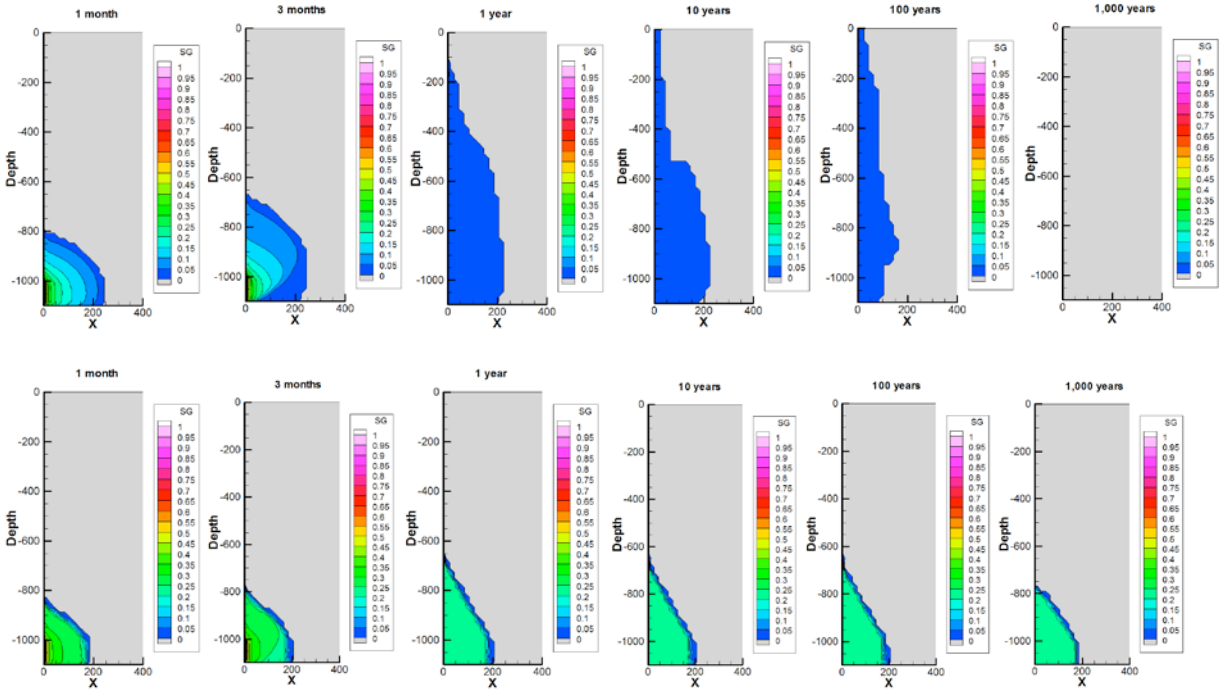

Figure 8. Nonhysteretic simulations with S_{gr} = 0 (on top) and S_{gr} = 0.25 (on bottom).

Figure 9 shows the results of Doughty's simulation and our simulation using hysteretic characteristic curves. Both models predict CO_2 plumes of an intermediate mobility compared to the nonhysteretic simulations. Doughty's model predicts a slightly more mobile CO_2 plume than our model predicts; seen at 10 and 100 years, where the 5% CO_2 saturation contour reaches a depth of about 500 m for Doughty's simulation and a depth of about 600 m for our simulation. The new model predicts a CO_2 plume of similar shape to Doughty's model, and the final snapshot at 1,000 years shows a comparable size of CO_2 plume. The simulation results compare favorably and confirm that the new and simplified hysteretic CO_2 trapping function is able to reproduce the essential features of a more complicated hysteretic model.

The CO_2 saturation for the four simulations is plotted as a function of time at a depth of 700 m on the radial center of the grid (figure 10). The four models predict the highest CO_2 saturations at early simulation time, then variable behavior as simulation time progresses. The nonhysteretic high S_{gr} case retains CO_2 saturation around 25% for most of the simulation, but at 700 m of depth on the radial center, the CO_2 saturation drops to

0 over time due to dissolution of the CO_2 phase. The nonhysteretic low S_{gr} case predicts that CO_2 saturation quickly drops to 0 due to the lack of trapping. The two hysteretic cases show predictions of CO_2 saturation with intermediate behavior, but complete CO_2 dissolution by the 1,000-year simulation time.

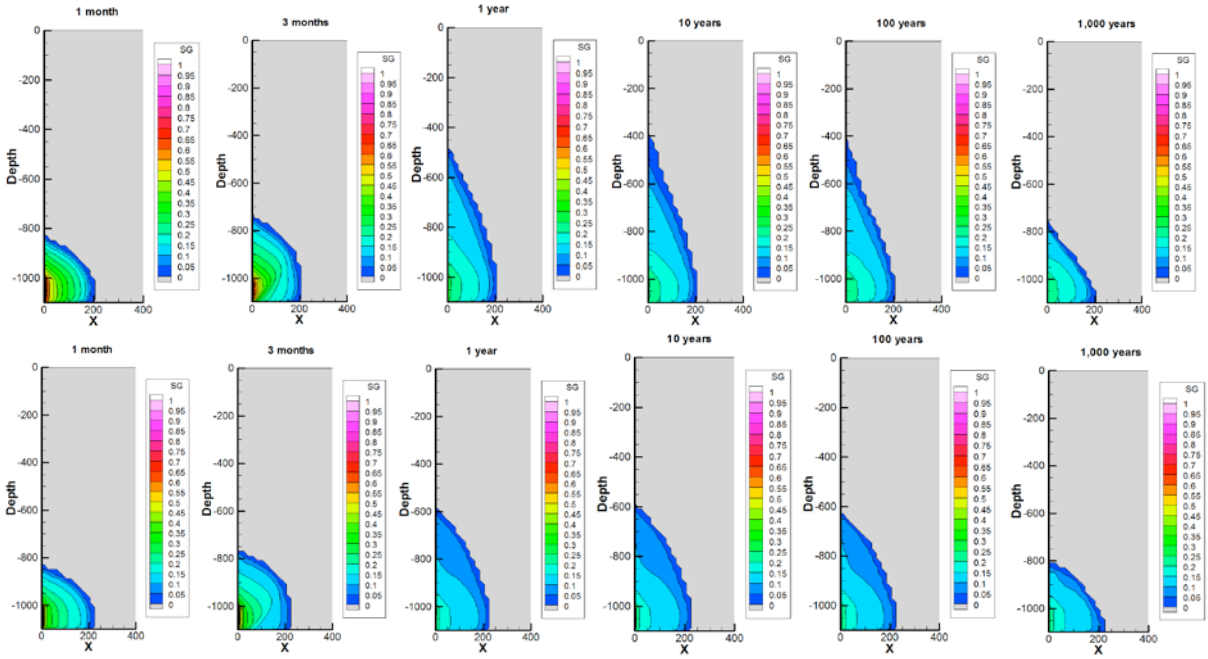

Figure 9. Simulation results from Doughty (2007) on top, and the new hysteretic simulation on bottom.

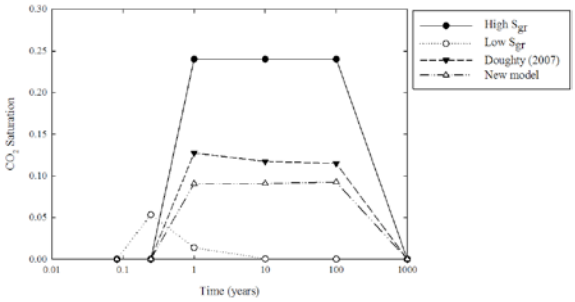

Figure 10. Plot of CO_2 saturation over time at a depth of 700 m at the radial center of the simulation grid.

CONCLUSION

The use of hysteretic characteristic curves greatly impacts the results of numerical simulations of multiphase flow by controlling the mobility of the fluids. For problems with significant nonwetting-phase trapping, the most important part of a hysteretic characteristic curve may be the variable value of residual saturation, which represents the saturation of the nonwetting phase that has become immobilized due to capillary forces.

A new, efficient, and straightforward hysteretic model is described to implement the history-dependent trapping processes during multiphase flow simulations. The numerical nature of the new model ensures continuously differentiable saturation turning points, which eases performance in numerical simulators. An advantage of this new method of tracking hysteresis in the multiphase flow characteristic curves is the fact that there is no need for additional characteristic curve parameters. The new hysteretic model is capable of irreversible saturation paths using the same number of parameters that a simple non-hysteretic model would employ.

The new model was assessed by comparison to experimental results and published simulation results. The results confirm that the new model performs favorably and is capable of reproducing the essential features of more complex hysteretic models used for multiphase modeling.

ACKNOWLEDGEMENTS

We would like to thank Christine Doughty and Colin Johnston for their contributions to this

project. This work was funded by U.S. EPA STAR Grant #834383. Publication authorized by the Director, Illinois State Geological Survey.

REFERENCES

Alley, R., T. Berntsen, N.L. Bindoff, Z. Chen, A. Chidthaisong, P. Friedlingstein, J. Gregory,G. Hegerl, M. Heimann, B. Hewitson, B. Hoskins, F. Joos, J. Jouzel, V. Kattsov, U. Lohmann, M. Manning, T. Matsuno, M. Molina, N. Nicholls, J. Overpeck, D. Qin, G. Raga, V. Ramaswamy, J. Ren, M. Rusticucci, S. Solomon, R. Somerville, T.F. Stocker, P. Stott, R.J. Stouffer, P. Whetton, R.A. Wood, D. Wratt, 2007, Climate change 2007: The physical science basis, Summary for policymakers, IPCC WGI Fourth Assessment Report, Intergovernmental panel on climate change, Cambridge University Press, Cambridge, U.K.

Charbeneau, R., 2007, LNAPL Distribution and Recovery Model (LDRM) Volume 1: Distribution and Recovery of Petroleum Hydrocarbon Liquids in Porous Media, American Petroleum Institute API Publication 4760.

Doughty, C., 2007, Modeling geologic storage of carbon dioxide: comparison of non-hysteretic and hysteretic characteristic curves, Energy Conversion and Management, 48, 1768-1781.

Doughty, C., 2010, personal communication with Christine Doughty.

Fagerlund, F., A. Niemi, and T.H. Illangasekare, 2008, Modeling of nonaqueous phase liquid (NAPL) migration in heterogeneous saturated media: Effects of hysteresis and fluid immobility in constitutive relations, Water Resources Research, 44, W03409.

Falta, R.W., K. Pruess, S. Finsterle, and A. Battistelli, 1995, T2VOC user's guide, Rep. LBL-36400, Lawrence Berkeley National Laboratory, Berkeley, California.

Johnston, C., and M. Adamski, 2005, Relationship between initial and residual LNAPL saturation for different soil types, Proceedings of the 2005 Petroleum Hydrocarbons and Organic Chemicals in Groundwater®: Prevention, Assessment, and Remediation Conference. 17-19 August, Costa Mesa, 29-42.

Johnston, C., 2010, personal communication with Colin Johnston.

Juanes, R., E.J. Spiteri, F.M. Orr Jr., and M.J. Blunt, 2006, Impact of relative permeability hysteresis on geological CO_2 storage, Water Resources Research, 42, W12418.

Juanes, R., C.W. MacMinn, and M.L. Szulczewski, 2010, The footprint of the CO_2 plume during carbon dioxide storage in saline aquifers: storage efficiency for capillary trapping at the basin scale, Transp Porous Med, 82, 19-30.

Kaluarachchi, J.J., and J.C. Parker, 1992, Multiphase flow with a simplified model for oil entrapment, Transport in Porous Media, 7, 1-14.

Krevor, S.C.M., R. Pini, B. Li, and S.M. Benson, 2011, Capillary heterogeneity trapping of CO_2 in a sandstone rock at reservoir conditions, Geophysical Research Letters, 38: L15401.

Kueper, B.H., D. Redman, R.C. Starr, S. Reitsma, and M. Mah, 1993, A field experiment to study the behavior of tetrachloroethylene below the water table: spatial distribution of residual and pooled DNAPL, Ground Water, 31: 5, 756-766.

Land, C. S., 1968, Calculation of imbibition relative permeability for two- and three-phase flow from rock properties, Transactions, 243, 149-156.

Lenhard, R.J., and J.C. Parker, 1987, A model for hysteretic constitutive relations governing multiphase flow: 2. Permeability-saturation relations, Water Resources Research, 23:10, 2197-2206.

Lenhard, R.J., and J.C. Parker, 1987, Measurement and prediction of saturation-pressure relationships in three-phase porous media systems, Journal of Contaminant Hydrology, 1, 407-424.

Lenhard, R.J., 1992, Measurement and modeling of three-phase saturation-pressure hysteresis, Journal of Contaminant Hydrology, 9, 243-269.

Mayer, A.S., and S.M. Hassanizadeh (Eds.) (2005), *Soil and Groundwater Contamination: Nonaqueous Phase Liquids–Principles and Observations*, Water Resour. Monogr. Ser., vol. 17, 216 pp., AGU, Washington, D.C., doi: 10.1029/WM017.

Mualem, Y., 1976, A new model for predicting the hydraulic conductivity of unsaturated porous media, Water Resources Research, 12:6, 513-522.

Mualem, Y., 1984, A modified dependent-domain theory of hysteresis, Soil Science, 137:5, 283-291.

NETL, 2007, Carbon Sequestration Atlas of the United States and Canada, U.S. Department of Energy, National Energy Technology Laboratory. Available from http://www.netl.doe.gov/technologies/carbon_seq/refshelf/atlas/ATLAS.pdf

Niemi, A., and G.S. Bodvarsson, 1988, Preliminary capillary hysteresis simulations in fractured rocks, Yucca Mountain, Nevada, Journal of Contaminant Hydrology, 3, 277-291.

Parker, J.C., and R.J. Lenhard, 1987, A parametric model for constitutive properties governing multiphase flow in porous media, Water Resources Research, 23: 4, 618-624.

Patterson, C.G., 2011, A history-dependent nonwetting phase trapping model for multiphase flow characteristic curves, Master's thesis, Clemson University.

Pruess, K., C. Oldenburg, and G. Moridis, 1999, TOUGH2 user's guide, version 2.0, Rep. LBNL-43134. Berkeley: Lawerence Berkeley National Laboratory.

Pruess, K. and A. Battistelli, 2002, TMVOC, A numerical simulator for three-phase non-isothermal flows of multicomponent hydrocarbon mixtures in saturated-unsaturated heterogeneous media, LBNL-49375, Lawrence Berkeley National Laboratory, Berkeley, CA.

Pruess, K., 2005, ECO2N: A TOUGH2 fluid property module for mixtures of water, NaCL, and CO_2, LBNL-57952, Earth Sciences Division, Lawrence Berkeley National Laboratory, University of California, Berkeley, CA.

Saadatpoor, E., S.L. Bryant, and K. Sepehrnoori, 2009, Effect of capillary heterogeneity on buoyant plumes: a new local trapping mechanism, GHGT-9, Energy Procedia 1, 3299-3306.

Suekane, T., N.H. Thanh, T. Matsumoto, M. Matsuda, M. Kiyota, A. Ousaka, 2009, Direct

measurement of trapped gas bubbles by capillarity on the pore scale, GHGT-9, Energy Procedia 1, 3189-3196.

Steffy, D.A., D.A. Barry, and C.D. Johnston, 1997, Influence of antecedent moisture content on residual LNAL saturation, Soil and Sediment Contamination: An International Journal, 6: 2, 113-147.

Van Geel, P.J., and S.D. Roy, 2002, A proposed model to include a residual NAPL saturation in a hysteretic capillary pressure-saturation relationship, Journal of Contaminant Hydrology, 58, 79-110.

van Genuchten, M.T., 1980, A closed-form equation for predicting the hydraulic conductivity of unsaturated soils, Soil Sci. Soc. Am. J., 44, 892-898.

van Genuchten, M.T. and D.R. Nielsen, 1985, On describing and predicting the hydraulic properties of unsaturated soils, Annales Geophysicae, 3:5, 615-628.